Received: 16 April 2019 | Revised: 8 December 2019 | Accepted: 15 December 2019
DOI: 10.1002/we.2476

WILEY

RESEARCH ARTICLE

On design, modelling, and analysis of a 10-MW medium-speed drivetrain for offshore wind turbines

Shuaishuai Wang[1] | Amir R. Nejad[1] | Torgeir Moan[1,2]

[1]Department of Marine Technology, Norwegian University of Science and Technology (NTNU), Trondheim, Norway
[2]Center of Autonomous Marine Operations and Systems (AMOS), NTNU, Trondheim, Norway

Correspondence
Shuaishuai Wang, Department of Marine Technology, Norwegian University of Science and Technology (NTNU), Trondheim NO-7491, Norway.
Email: shuaishuai.wang@ntnu.no

Funding information
China Scholarship Council (CSC), Grant/Award Number: 201706050147

Abstract

The design of a medium-speed drivetrain for the Technical University of Denmark (DTU) 10-MW reference offshore wind turbine is presented. A four-point support drivetrain layout that is equipped with a gearbox with two planetary stages and one parallel stage is proposed. Then, the drivetrain components are designed based on design loads and criteria that are recommended in relevant international standards. Finally, an optimized drivetrain model is obtained via an iterative design process that minimizes the weight and volume. A high-fidelity numerical model is established via the multibody system approach. Then, the developed drivetrain model is compared with the simplified model that was proposed by DTU, and the two models agree well. In addition, a drivetrain resonance evaluation is conducted based on the Campbell diagrams and the modal energy distribution. Detailed parameters for the drivetrain design and dynamic modelling are provided to support the reproduction of the drivetrain model. A decoupled approach, which consists of global aero-hydro-servo-elastic analysis and local drivetrain analysis, is used to determine the drivetrain dynamic response. The 20-year fatigue damages of gears and bearings are calculated based on the stress or load duration distributions, the Palmgren-Miner linear accumulative damage hypothesis, and long-term environmental condition distributions. Then, an inspection priority map is established based on the failure ranking of the drivetrain components, which supports drivetrain inspection and maintenance assessment and further model optimization. The detailed modelling of the baseline drivetrain model provides a basis for benchmark studies and support for future research on multimegawatt offshore wind turbines.

KEYWORDS

10-MW medium-speed drivetrain, decoupled analysis, fatigue damage, inspection map, model design, offshore wind turbine

1 | INTRODUCTION

In the past decade, the number of offshore wind turbine installations has increased rapidly. Meanwhile, the offshore wind turbine size has been upscaled as this appears to be an effective solution for reducing the levelized cost of wind power. A concept description of a 10-MW wind turbine was proposed by Technical University of Denmark (DTU) in 2013.[1] Since then, many studies[2-4] have been conducted on the design and dynamic analysis of the 10-MW reference wind turbine (RWT). However, all these studies are focused on the blades and tower; thus far, no studies have examined the 10-MW wind turbine drivetrain.

According to the peer-reviewed literature on the wind turbine drivetrain study, only limited drivetrain or gearbox models are found being publicly available for communicative and cooperative study; however, they have given rise to substantial outcomes. A 750-kW baseline wind turbine gearbox that was provided from the gearbox reliability collaborative (GRC) project by the National Renewable Energy Laboratory (NREL) has been used in various studies. Guo et al[5] established the 750-kW drivetrain multibody dynamic model and investigated the combined effects of gravity, the bending moment, the bearing clearance, and the input torque on the planetary load sharing performance. Dong et al[6] proposed

The peer review history for this article is available at https://publons.com/publon/10.1002/we.2476

a simplified predictive pitting model, which is used to estimate the contact fatigue life of gears in the 750-kW drivetrain model. Considering normal operation and parked and transient load cases, a long-term contact fatigue analysis of a planetary rolling element bearing in the 750-kW drivetrain was conducted by Jiang et al.[7] Xing et al[8] studied the dynamics of the 750-KW wind turbine drivetrain supported on a spar-type floating structure, and the dynamic response in the floating wind turbine was compared with that in its equivalent land-based version. Additionally, an offshore gearbox was designed by Nejad et al[9] for the NREL 5MW baseline wind turbine, and they provided detailed descriptions, modelling parameters, and technical data to the public to support research studies for large offshore wind turbines.

However, almost all of these drivetrain models are equipped with the high-speed gearboxes. Very limited studies have been conducted on the medium-speed drivetrains because of the lack of an available reference model. Faced with a reliability problem for the commonly used high-speed drivetrain and a weight issue for the direct-driven drivetrain in the wind turbine upscaling procedure, the medium-speed drivetrain, which is typically composed of a simplified gearbox with only one or two stages and a medium-speed electric generator, is being regarded as a potential alternative in offshore applications. This is because the medium-speed drivetrain could have the advantages of both the high-speed and the direct-driven drivetrain concepts: It could possibly lower the risk of gearbox failure compared with the high-speed drivetrain, while reducing the generator's weight and cost compared with the direct-driven drivetrain. A few applications of the medium-speed drivetrain have been found in large-scale offshore wind turbines in recent years, such as AREVA M[10] Vestas EnVentus V162-5.6 MW,[11] MHI VestasV174-9.5 MW, and V164-10.0 MW.[12] The DTU 10-MW RWT was also proposed to equip with a medium-speed drivetrain, but no related design has been reported in the literature.

The objective of this study is to improve communication and cooperation between various stakeholders to enhance research studies on large-scale offshore wind turbines. To realize this objective, a medium-speed drivetrain is designed for the DTU 10-MW RWT. Detailed design descriptions, including the design basis, loads, criteria, and principles, are presented. Then, a drivetrain numerical model is established via the multibody system modelling method, and the suitability of the modelling parameters is demonstrated via comparative analysis between the developed model and the simplified model that is provided by DTU and by conducting a drivetrain resonance evaluation. Sufficient drivetrain design and dynamic modelling parameters are provided, thereby rending the drivetrain model to be reproducible. Thus, one can replicate the drivetrain model that is utilized in their work to gain insight into the dynamics of 10-MW wind turbines. Moreover, the 20-year drivetrain fatigue damage is calculated using gear and bearing loads that are obtained from the dynamic simulations, the linear fatigue cumulative damage hypothesis, and the long-term environmental condition distributions. Then, a drivetrain vulnerability map is then established by ranking the fatigue damage from the highest to lowest, which supports drivetrain performance assessment and design improvement.

2 | WIND TURBINE DESCRIPTION

2.1 | Wind turbine specifications

The DTU 10-MW RWT that serves as the drivetrain design in this study was designed by upscaling the NREL 5 MW reference wind turbine,[13] which is characterized by an efficient lightweight rotor and a medium-speed drivetrain. An overall description of the 10-MW wind turbine is presented in Table 1. The wind turbine was designed for offshore sites with an International Electrotechnical Commission (IEC) class 1A wind climate and is a traditional three-bladed, upwind wind turbine with a variable-speed collective pitch power control system.[1]

2.2 | Drivetrain properties

The general parameters of the drivetrain that were proposed by DTU are listed in Table 2. These parameters are only used for the simplified drivetrain modelling, namely, for the torsional model with one degree of freedom (DOF) in the global analysis. A detailed drivetrain model is not offered by DTU.

TABLE 1 Key parameters of the DTU 10-MW reference wind turbine[1]

Parameter	Value
Rated power (MW)	10
Cut in wind speed (m/s)	4
Rated wind speed (m/s)	11.4
Cut out wind speed (m/s)	25
Rotor diameter (m)	178.3
Hub height (m)	119.0
Hub diameter (m)	5.6
Drivetrain	medium-speed, multiple stage gearbox
Hub overhang (m)	7.1
Shaft tilt angle (deg)	5.0
Rotor mass (kg)	227962
Nacelle mass (kg)	446036
Tower mass (kg)	628442

Parameter	Value
Gearbox ratio	1:50
Minimum rotor speed (rpm)	6.0
Rated rotor speed (rpm)	9.6
Rated generator speed (rpm)	480.0
Electrical generator efficiency	94
Generator inertia about high-speed shaft (kgm^2)	1500.5
Equivalent drive-shaft torsional-spring constant (Nm/rad)	2317025352
Equivalent Drive-Shaft torsional-damping constant (Nm/(rad/s))	9240560
Natural frequency of free-free rigid shaft torsion mode	4.003
Natural frequency of free-fixed rigid shaft torsion mode	0.612

TABLE 2 Drivetrain properties proposed by DTU[1]

3 | METHODOLOGY

3.1 | Environmental conditions, global response, and local drivetrain response analysis

In this study, the 10-MW wind turbine drivetrain is selected to be supported on a bottom-fixed monopile offshore structure. According to the study of Nejad et al,[14] wave loads have very limited effects on the dynamic response of a drivetrain with this type of offshore structure support. Thus, in this study, the influences of wave loads on the drivetrain design and on the analysis are neglected, and wind loads are considered to be the only environmental loads. An offshore field in the Northern North Sea is considered as the wind turbine installation site, where hindcast data have been sampled hourly for the wind speed. The long-term 1-hour mean wind speed at 10 m above the average sea level is modelled by a two-parameter Weibull distribution[15,16]:

$$F_U(u) = 1 - exp\left(-\left(\frac{u}{a}\right)^c\right), \tag{1}$$

where u is 1-hour mean wind speed at 10 m above the average sea level; a and c are the shape and scale parameters, which are 8.426 and 1.708, respectively.[15]

A power law is used to calculate wind speed at hub height:

$$u_{hub} = u\left(\frac{h_{hub}}{10}\right)^{\alpha}, \tag{2}$$

where h_{hub} is the hub height, which is 119 m above the average sea level for this 10-MW reference wind turbine; α is the power law exponent, which is assumed to be 0.14 for offshore fields as proposed in the international standard IEC 61400-3.[17]

A two-step decoupled analysis approach is employed in this study. First, a global response analysis of the 10-MW wind turbine that is equipped with a simplified drivetrain is conducted using an aero-hydro-servo-elastic dynamic software, namely, SIMA.[18] Then, the rotor forces and moments and the nacelle motions that are obtained from the global analysis are applied to the detailed drivetrain model to conduct a dynamic analysis. Compared with fully coupled analysis approach that solves for the drivetrain's dynamic response in a full wind turbine model, such a decoupled method could realize higher efficiency with less computation time and reasonable accuracy of the numerical results. Detailed descriptions of the decoupled method for the drivetrain response analysis can be found in other studies.[6,19,20]

3.2 | Drivetrain design methodology

3.2.1 | Drivetrain design basis

The 10-MW drivetrain is designed based on the international standard IEC 61400-4.[21] This standard accounts for the wind turbine gearbox design requirements and is applicable for horizontal-axis wind turbines with a power rating in excess of 500 KW in both onshore and offshore fields. The drivetrain design lifetime, design loads, interfaces definition, and specific design codes for the mechanical components are documented in IEC 61400-4,[21] which provide the main guidance and basis for the drivetrain design in this case study.

3.2.2 | Drivetrain design loads

According to the descriptions of the wind conditions in the international standards IEC 61400-1[22] and DNVGL-ST-[23] and to the study of Jiang et al,[7] normal operational conditions are the most important for the wind turbine drivetrain design and dynamic analysis. Thus, drivetrain design loads are derived from normal wind conditions, where design load case DLC 1.2 in IEC 61400-1[22] is applied in this study.

The design load spectra are generated by processing the time series of rotor blade loads that are obtained from the global simulation, which is conducted under normal operational conditions that cover the whole range from the cut-in to cut-out speed. The torque load duration distribution (LDD) is shown in Figure 1, which consists of 64 load bins, and the total duration time is 1.67e5 hours, which corresponds to a 20-year service life with 95% availability of power production. Other nontorque LDDs, which are not presented in this paper, are also considered for the drivetrain design. These nontorque LDDs have limited effects on the sizing of the mechanical components inside the gearbox, while account largely for the main bearing design.

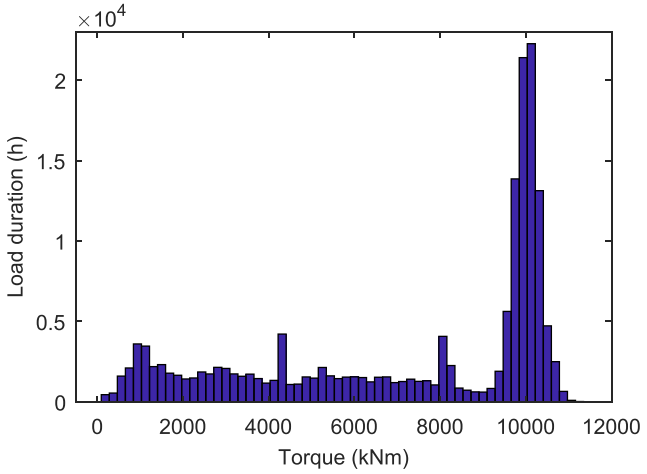

FIGURE 1 Design load duration distribution of wind turbine drivetrain in 20 years [Colour figure can be viewed at wileyonlinelibrary.com]

3.2.3 | Drivetrain configuration and gearbox layout

Among the currently available geared drivetrain designs, the drivetrain configurations can be divided into three main categories: three-point suspension, two-main-bearing suspension, and integrated drivetrain. Based on industry experiences and a related study[24] on the feasibility of various drivetrain configurations in modern large offshore wind turbines, a four-point support drivetrain configuration with two main bearings and two torque arms is applied in this study.

A conventional high-speed gearbox is typically composed of three stages, namely, one planetary stage and two parallel stages or two planetary stages and one parallel stage, with total transmission ratio of approximately 80:1 to 120:1, while the transmission ratio of the DTU 10-MW medium-speed wind turbine gearbox is 50:1. According to the industry experiences, the medium-speed gearbox is typically designed with one or two stages with the objective of reducing the gearbox failure rate by eliminating the high speed part, which is considered as the main source of gearbox failure. However, according to the study of Schmidt et al,[25] the conventional two planetary stages gearboxes are facing the design limit restrictions with a maximum transmission ratio of approximately 40. For addressing this gear ratio restriction, several potential solutions are proposed and discussed in the following.

The most reliable and simple solution is to adopt the conventional three-stage design of which the layout with two planetary stages and one parallel stage could be feasible in this case study. Although the layout is the same as that of the high-speed gearbox, the gearbox failure rate and failure modes might differ. According to the studies of Guo et al,[26,27] most gearbox premature failures occur on the intermediate- and high-speed shaft bearings, with a primary failure mode of axial cracks or white etching cracks (WECs), which might be caused by factors such as electrical current, hydrogen embrittlement, impact loading, and roller/raceway sliding. However, the loads and speeds that are experienced by the intermediate- and high-speed shafts in the medium-speed gearbox differ from those in the high-speed gearboxes; thus, the influences of those factors on the bearing fatigue damage could differ. Moreover, a promising solution is to replace the classical planetary gearbox with a novel layout such as a power splitting gearbox, a compound, differential or double-helix planetary gearbox, or a combination of them. These novel layouts have enormous potential as they not only realize a high gear ratio but also result in a more compact gearbox with lighter weight and smaller volume, which yields a higher torque or power density compared with the conventional layouts, which was demonstrated in another studies[28,29] of the authors. However, these novel technologies have not been widely used, namely, the applicability of these gearbox concepts may have yet to be reasonably evaluated. This is because there is currently a lack of deep understanding of the dynamic behaviors and reliability of the novel gearbox concepts because of the effects of structure flexibility, stiffness, damping, and multiple source errors. Moreover, the manufacturing, installation, maintenance, and repair procedures of the novel concepts have not been properly estimated. This is because the highly accurate design requirements pose huge difficulties in their manufacturing and assembly, and some of the mechanical components might need to be custom made. In addition, the compact gearbox typically has less available space, which is unfavourable for inspection, maintenance, and repair. Hence, costs have not been estimated accurately.

Compared with the novel gearbox layouts, the conventional three-stage gearbox is more feasible according to many studies on design, dynamic analysis, and cost estimation that have been conducted. As the objective of this study is to provide support for cooperative and comparative studies to facilitate research on the dynamics of 10-MW offshore wind turbines, the conventional three-stage gearbox seems to be more suitable as a baseline model for the present target; thus, this layout is selected to be designed in this study.

3.2.4 | Drivetrain component design

The main components of the drivetrain include hub, mainshaft, main bearing, gearbox, coupling, generator, and bedplate. The geometries of the hub, the mainshaft, the coupling, the generator, and the bedplate are designed by referring to the corresponding components in a 2-MW land-based wind turbine, as presented by Wang et al.[30]

The basic flow of the gearbox components sizing process is presented in Figure 2. All components are designed based on gearbox design LDD and following the design requirements that are defined in the international standard IEC 61400-4.[21] Gears are designed based on the

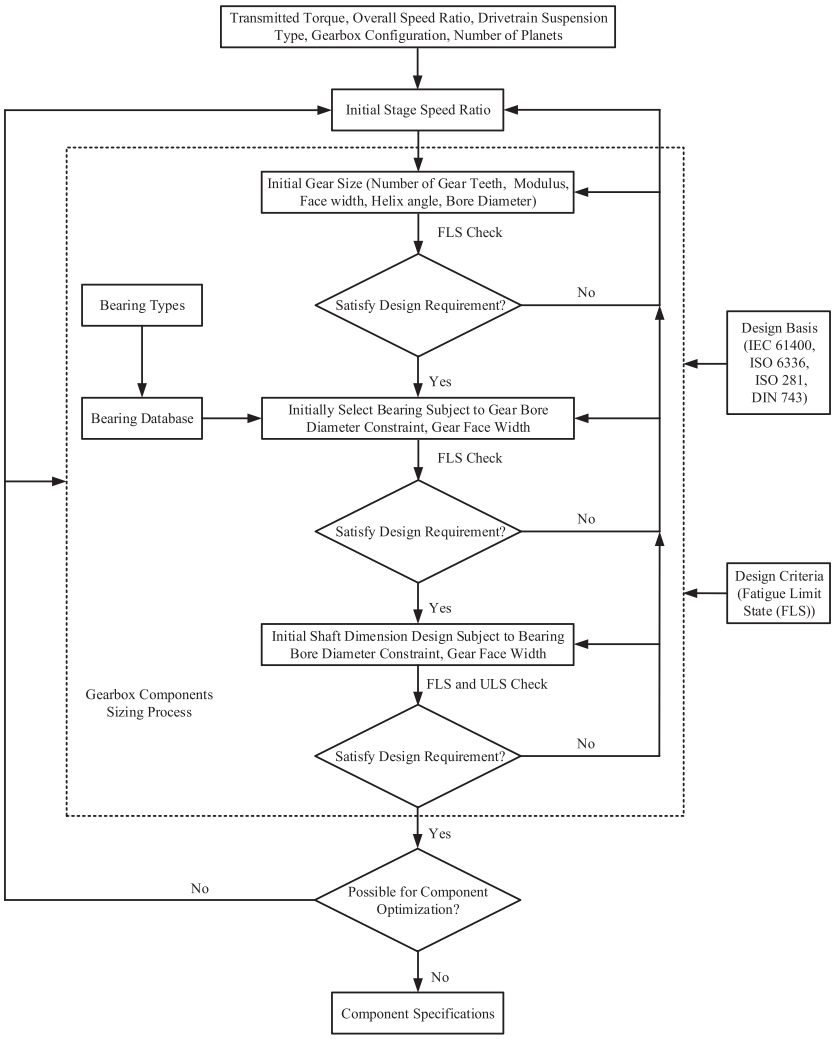

FIGURE 2 Flowchart of the gearbox components sizing process

international standards ISO 6336-2,[31] ISO 6336-3,[32] and ISO 6336-6.[33] Gear carrying loads and load capacities are calculated according to these design standards, and the safety factors that are recommended in IEC 61400-4[21] are used to guide the gear design. Bearings are designed based on the international standard ISO 281[34] in which the bearing dynamic load rating and the basic rating life are calculated. Then, the bearing lifetime for the given LDD is used to guide the design. The process is described in detail in the reference Wang et al.[29] Moreover, fatigue analysis of the shafts is conducted according to the standard DIN 743,[35] and the shafts are designed by referring to the minimum safety factors that are recommended in this standard.

First, the gearbox initial gear ratio in each stage is set with determined drivetrain information such as the rated torque, the overall speed ratio, and the gearbox configuration. Then, the initial gear size, which is determined by parameters such as the number of gear teeth, the gear modulus, and the face width, is calculated based on the gear load rating. Next, the initial bearing size is selected based on the gear bore diameter and the gear face width constraint. The bearing type selection and arrangements are determined by referring the IEC 61400-4[21] recommendation and the 5-MW offshore wind turbine gearbox design case.[9] The bearing designation is chosen from the bearing database in software KISSsoft[36] with the determined bearing size and type. Next, the initial shaft dimension is designed according to the bearing bore diameter and the gear face width. This component's sizing design flow is compatible with the planetary stage, while for the main shaft and parallel stage components design, the initial shaft dimension is determined after the gear design and is followed by bearing selection. If all components satisfy the safety requirements that are specified in the relevant design codes, the components are optimized by reducing the component material and enabling the component strength to be close to the safety limit. The component specifications are eventually obtained via an iterative sizing and optimization process. KISSsoft 2018 was used for the component sizing.

Four gearbox layout options are proposed and are designed using the gearbox flowchart that is presented above. The design results are presented and compared in Table 3. Compare with the options A and B, a more compact gearbox can be realized by the options C and D. While the option D is slightly smaller and lighter than the option C, it has a higher requirement on the gearbox load-sharing performance. Based on this, the option C is eventually selected in this case study. A detailed analysis is described in the study of Wang et al.[37]

TABLE 3 Four gearbox layout design options

Parameter	A	B	C	D
First stage	1:6.000 (3p)	1:5.280 (4p)	1:4.423 (5p)	1:3.316 (6p)
Second stage	1:5.348 (3p)	1:5.160 (3p)	1:5.192 (3p)	1:5.625 (3p)
Third stage	1:1.556	1:1.826	1:2.179	1:2.680
Total gear ratio	1:49.929	1:49.749	1:50.039	1:49.989
Total dry weight (×1000kg)	65.66	60.59	60.43	57.16
Maximum outer diameter (m)	3.878	3.396	3.098	3.068

Abbreviation: p, planets.

3.3 | Drivetrain numerical modelling

In this study, the wind turbine drivetrain is modelled numerically via a multibody system (MBS) approach. The multibody drivetrain model is composed of various rigid and flexible bodies, which are connected by kinematic constraints. SIMPACK,[38] which is a general-purpose MBS software that is widely used for the kinematics and dynamic analyses of complex mechanical systems, is employed for the drivetrain dynamic modelling in this study. The basic modelling elements in SIMPACK are ''body'', ''joint,'' and ''force element,'' where ''body'' represents the drivetrain component, and the ''joint'' and ''force element'' are used to define the connections among components. The dynamic behaviour of the drivetrain model could be obtained by solving for the system motions with the applied forces and the body inertia. The simulation software has been successfully used for modelling and dynamic analysis on wind turbine drivetrains, as presented in earlier studies.[39-41]

Many studies[42-44] have demonstrated that the complexity of the components strongly influences the dynamic behaviours of the wind turbine drivetrain. A high-fidelity numerical model that consists of flexible bodies can capture the dynamic behaviours accurately; however, the simulation process is time-consuming. To compromise between the accuracy of the dynamic behaviours and computation time, a rigid-flexible coupled drivetrain model is established in this study. Based on the minimum requirements for drivetrain component modelling that are described in international standard DNVGL-ST-[23] and the recommendation of Guo et al,[45] the mainshaft, planet carriers, and transmission shafts in the gearbox are represented by flexible bodies, and the hub, bedplate, housing, and gears are modelled as rigid bodies in this study.

In SIMPACK, each gear tooth contact is modelled by a force element, namely, FE 225, and the contact force is composed of stiffness, damping, and friction terms, where the gear meshing stiffness is modelled by a series of spring elements along the line of action, and the stiffness value of each spring element is calculated based on the standard ISO 6336-1.[46]

Bearings are modelled by force element FE 43 with a linear force-deflection relationship in SIMPACK. In this paper, the bearing stiffness is represented as a linear diagonal stiffness as follows:

$$\mathbf{K} = \begin{pmatrix} K_{xx} & 0 & 0 & 0 & 0 & 0 \\ & K_{yy} & 0 & 0 & 0 & 0 \\ & & K_{zz} & 0 & 0 & 0 \\ & & & K_{\alpha\alpha} & 0 & 0 \\ & sym. & & & K_{\beta\beta} & 0 \\ & & & & & K_{\gamma\gamma} \end{pmatrix}, \tag{3}$$

where K_{xx}, K_{yy}, and K_{zz} represent the axial, tangential, and radial stiffness, respectively, with units in N/m. The $K_{\beta\beta}$ and $K_{\gamma\gamma}$ represent pitch and yaw stiffness, respectively, with unit in Nm/rad. The $K_{\alpha\alpha}$ is 0, because α corresponds to rotation direction. The coupling effects between different DOFs are not considered in this study, so the off-diagonal terms are zeros. The bearing stiffness is calculated using the software Romax.[47]

The generator is modelled by a proportional-integral velocity controller that is applied on the generator shaft. The velocity controller uses the generator angular velocity that is obtained from the global analysis as a reference; then, the generator torque, which is denoted as T_{Gen}, is calculated via the following equation[9]:

$$T_{Gen} = K_P + K_I \int_0^t (w - w_{ref})dt, \tag{4}$$

where w is the generator angular velocity calculated in the drivetrain model, and w_{ref} is the reference value obtained from global simulation. K_P and K_I are proportional and integral gain, respectively. In each simulation time step, T_{Gen} is calculated and applied on the generator shaft.

3.4 | Gear fatigue damage calculation

The long-term gear bending and pitting fatigue damage are calculated in this study. First, the gear tooth contact and bending stresses are calculated by postprocessing the time-varying gear transmitted loads that are obtained from the drivetrain MBS simulation, according to the methods that are proposed in manuals ISO 6336-2[31] and ISO 6336-3,[32] respectively. Then, gear tooth stress bins are created using a stress cycle counting method, as demonstrated in the study of Nejad et al,[48] where the number of gear tooth stress cycles in each stress bin is calculated via the following equation:

$$n_i = \sum_j \frac{t_j w_j}{2\pi}, \tag{5}$$

where n_i is the number of stress cycles in the stress bin i, t_j is the j-th time duration of the bin i, and w_j is the average gear rotational speed (rad/s) in the j-th time duration of bin i. The numbers of stress cycles of the sun and ring gears are multiplied by 5 in the first stage and by 3 in the second stage because they mesh with several planets simultaneously and would encounter several (number of planets) contacts in each rotation.

For each wind speed, the 1-hour short-term gear bending and pitting fatigue damage are calculated according to the Palmgren-Miner linear accumulative damage hypothesis[49]:

$$D(u) = \sum_i \frac{n_i(u)}{N_i} = \frac{1}{k} \sum_i n_i(u) \cdot s_i^m, \tag{6}$$

where u represents the mean wind speed at the tower top height, $D(u)$ is the 1-hour accumulative gear fatigue damage at the wind speed u, n_i is the 1-hour number of cycles in stress bin i, and N_i is the permissible number of cycles in stress bin i, which is calculated by the gear design SN curve, namely, $N_i = k \cdot s_i^{-m}$, in which k and m are SN curve parameters that are calculated based on ISO 6336-2,[31] ISO 6336-3,[32] and ISO 6336-5.[50]

Long-term gear fatigue damage can then be calculated by[48]

$$D^{LT} = \int_{cut-in}^{cut-out} T \cdot D(u) \cdot f(u) \cdot du, \tag{7}$$

where T is 20-year gearbox design life, $f(u)$ is probability density function of mean wind speed.

3.5 | Bearing fatigue damage calculation

The bearing fatigue damage is calculated based on the Palmgren-Miner hypothesis. First, bearing basic rating life is calculated according to the load-life relationship, which is established via laboratory tests[34]:

$$L_{10} = \left(\frac{C}{P}\right)^a, \tag{8}$$

where L_{10} is the basic rating life, which is expressed units of 10^6 revolutions (r); L_{10} is defined as the number of cycles when 10% of the bearings in an identical group incur pitting damage while the remaining 90% bearings operate normally; C is the basic dynamic load rating, namely, the dynamic load that the bearing can withstand if the basic rating life is exactly 10^6 r, which is a specified constant for one bearing; P is the bearing dynamic equivalent load, which is calculated by $P = XF_r + YF_a$, where F_r and F_a are the radial loads and axial loads, respectively, that are experienced by the bearing, and X and Y are dynamic loading factors that are obtained from the bearing standard ISO 281; and a is the bearing life factor: For a ball bearing, $a = 3$, and for a roller bearing, $a = \frac{10}{3}$.

An each wind speed, the 1-hour bearing fatigue damage is calculated according to the linear accumulative damage hypothesis[51]:

$$D(u) = \sum_i \frac{l_i(u)}{L_i} = \frac{1}{c^a} \sum_i l_i(u) \cdot p_i^a, \tag{9}$$

where $D(u)$ is the 1-hour accumulative bearing fatigue damage at wind speed u; l_i is the 1-hour number of load cycles in load P_i, where l_i, which is associated with P_i, is calculated by employing the load cycle counting method, which is the same procedure that is used in the gear stress bin creation; and L_i is the permissible number of cycles in load P_i, which is calculated via Equation (8).

4 | RESULTS AND DISCUSSIONS

4.1 | Drivetrain specifications

4.1.1 | Drivetrain schematic layout

A schematic diagram of the 10-MW wind turbine layout is presented in Figure 3. According to the layout, the drivetrain is supported by two main bearings to prevent huge nontorque loads from entering the gearbox. A pair of tapered roller bearings are used as the main bearings, which is regarded as a promising application in large offshore turbines. This is because this bearing arrangement has satisfactory system stiffness and high reliability, and the short distance between the two bearings reduces the length of the main shaft, thereby making the drivetrain more compact. The specifications of the drivetrain model are listed in Table A1 in Appendix A.

4.1.2 | Component specifications

The drivetrain component specifications are listed in Appendix A. Table A2 presents the materials that were used in this study for the drivetrain component design. Table A3 lists the detailed gear geometrical specifications in which the gear profile shift coefficients are calculated by software KISSsoft based on the minimum slipping ratio principle. The detailed types, designations, and geometrical specifications of the bearings are listed in Table A4.

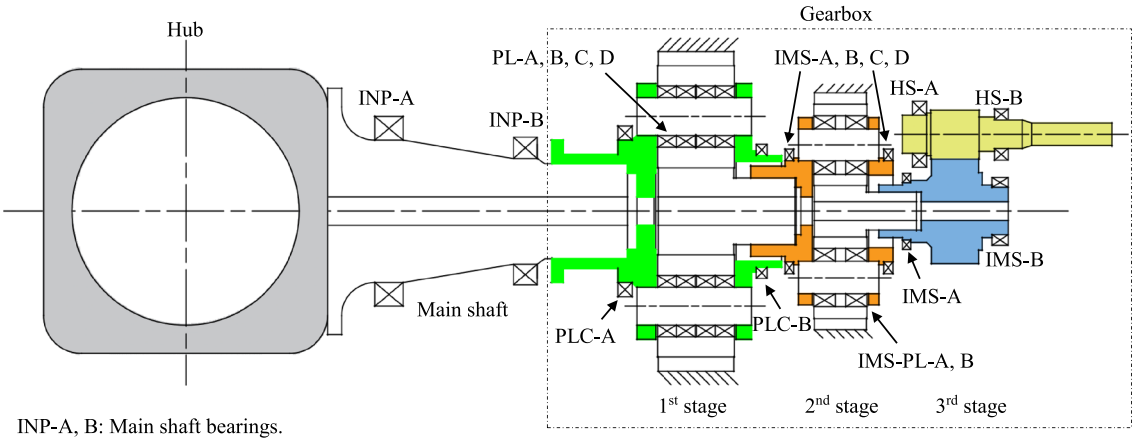

INP-A, B: Main shaft bearings.
PLC-A, B: Planet carrier bearing in the first stage; PL-A, B, C, D: Planet bearings in the first stage.
IMS-PLC-A, B: Planet carrier bearing in the second stage; IMS-PL-A, B: Planet bearings in the second stage.
IMS-A, B: Intermediate shaft bearings in the third stage; HS-A, B: High speed shaft bearings in the third stage.

FIGURE 3 10-MW wind turbine drivetrain schematic layout [Colour figure can be viewed at wileyonlinelibrary.com]

4.2 | MBS model and modelling parameters

The 10-MW drivetrain MBS model that is established using the SIMPACK software is illustrated in Figure 4. The connection relationships between the components in the MBS model and the DOFs of each element are illustrated in the drivetrain topological diagram in Figure B1 in Appendix B. The required parameters, such as the masses and the inertial moments of the components and the bearing modelling stiffness, for the drivetrain numerical modelling are presented in Tables B1 and B2. In this model, the mean contact stiffnesses of the gear pairs in the three stages are 1.4163×10^{10}, 9.9311×10^{9}, and 1.0215×10^{10} N/m, respectively.

4.3 | Model comparison

Since very limited drivetrain properties have been provided by DTU, many of the drivetrain modelling parameters that are assumed in this detailed model are associated with uncertainties, such as the torsional stiffness and the damping of the drivetrain components. An effective approach, which is proposed in the standard DNVGL-ST-[23] for evaluating the suitability of these parameters, is to compare the first eigenfrequencies between the detailed drivetrain model and the DTU simplified model. The first eigenfrequency of the simplified drivetrain model could be calculated via an equivalent mechanical equation, as specified by Nejad[52] and Oyague,[53] with the essential parameters that are presented in Table 2. Additionally, the first eigenfrequency of the detailed drivetrain model could be obtained by conducting modal analysis in SIMPACK. In the free-free drivetrain mode, the values that are calculated by the detailed and simplified drivetrain models are 3.889 and 4.003 Hz, respectively, and in the free-fixed mode, the values are 0.611 and 0.612 Hz, respectively. The first-order eigenfrequency in the simplified model accords with that in the detailed model, thereby suggesting that the drivetrain MBS modelling parameters could be reasonable.

4.4 | Resonance analysis of the drivetrain

Although the vibration modes of the drivetrain MBS model are multidimensional, this study focuses only on torsional vibration in which the resonance of the model is most likely to occur under dynamic excitation. The excitation frequencies of the drivetrain include shaft rotation frequencies and gear meshing frequencies that are within the normal operating speed range, which are listed in Table 4.

The natural frequencies that are obtained via modal analysis in SIMPACK are listed in Table 5. Since this analysis focuses on the drivetrain torsional modes, the frequencies that have no torsional mode shape are not listed in this table.

A Campbell diagram is plotted to screen the potential resonance points of the drivetrain model. The horizontal lines in the diagram correspond to natural frequencies and the oblique lines to excitation frequencies. The cross points in the diagram indicate the possible resonances in the

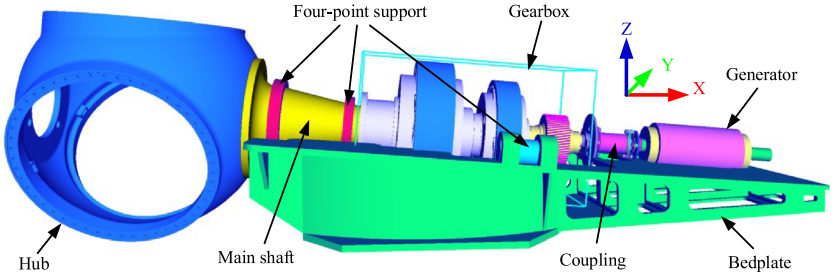

FIGURE 4 10-MW wind turbine drivetrain multibody system (MBS) model [Colour figure can be viewed at wileyonlinelibrary.com]

TABLE 4 Excitation frequencies of the drivetrain

Hub speed (rpm)	Minimum (6)	Maximum (9.6)
ms_1p	0.1	0.16
ms_2p	0.2	0.32
ms_3p	0.3	0.48
ms_6p	0.6	0.64
ims1	0.44	0.71
ims2	2.30	3.67
hss	5.00	8.01
st1_mesh	8.90	14.24
st2_mesh	48.21	77.14
st3_mesh	140.11	224.17

Note. ms_ip, main shaft rotation frequency; ims1/2, low/high speed intermediate shaft rotation frequency; hss, high speed shaft rotation frequency; stj_mesh, mesh frequency of the three stage gear pairs; where i means the ith order, p means harmonic and j means the jth stage.

TABLE 5 Natural frequencies of drivetrain in torsional mode

Order	f_N1	f_N2	f_N3	f_N4	f_N5	f_N6
Frequency (Hz)	3.889	6.294	73.177	144.591	175.412	206.754

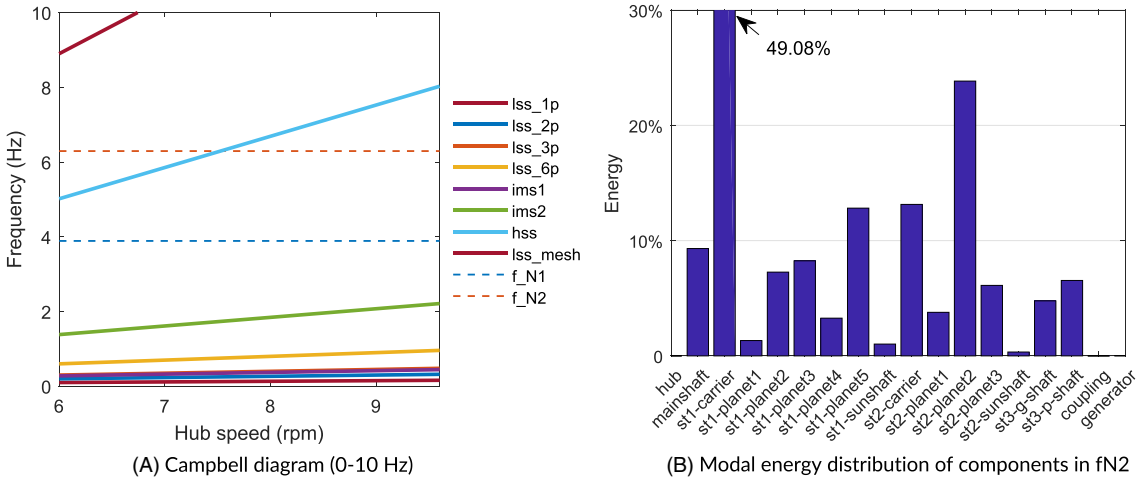

(A) Campbell diagram (0-10 Hz)

(B) Modal energy distribution of components in fN2

FIGURE 5 Campbell diagram and modal energy distribution
[Colour figure can be viewed at wileyonlinelibrary.com]

drivetrain model. To make the diagram clear and easy to interpret, the excitation frequencies are separated into three parts, which cover the whole excitation frequency range, and the first part (0-10 Hz), which is shown in Figure 5A, is considered as an example for demonstration in this study.

To further examine the possibility of resonance in this model, modal energy distributions of components that correspond to eigenfrequencies that have cross points with excitation frequencies are plotted. The modal energy calculation method is described in the study of Guo et al.[54] Figure 5B illustrates the modal energy distribution of components that correspond to eigenfrequency f_N2. The kinetic energy is mainly distributed on components st1_carrier and st2_planet2, which are selected based on the critical threshold of 20% energy, as recommended in international standard DNVGL-ST-0361.[23] However, the eigenfrequency f_N2 has a cross point with excitation frequency hss; hence, this frequency will not cause any resonance. The modal energy distribution of the components that correspond to each eigenfrequency is analysed via this approach, and the results demonstrate that resonance will not occur in this drivetrain model within the normal operating range.

4.5 | Drivetrain fatigue damage analysis and vulnerability map

Time-varying forces, moments, and nacelle motions that are calculated from the global simulation are applied for the drivetrain fatigue damage analysis. In the drivetrain model, the forces and moments that are produced by the rotor blades are applied at the hub centre; the generator feedback torque and speed are controlled on the generator rotor. Additionally, the nacelle motions are modelled by displacements, velocities, and accelerations and applied on the bedplate using the "joint" element in SIMPACK. To balance the computation time and the statistical uncertainties, eight simulations are conducted, which cover the wind speed range from 4 to 21 m/s, where each simulation time is set as 3800 s, and the first 200 s of data are removed to avoid start-up transient effects. The mean values and the standard deviations of the forces and moments, the nacelle motions, and the generator torque are plotted in Figures C1, C2, and C3, respectively, in Appendix C.

4.5.1 | Gear fatigue damage

Figure D1 in Appendix D plots the gear tooth bending and contact stress bins with the corresponding number of cycles for the first-stage sun gear at the wind speed of 12.6 m/s. The gear pitting and bending fatigue SN curve parameters, as listed in Table D1, are calculated based on the ISO 6336 standards, with the specified gear material and heat treatment. The 20-year gear tooth bending and pitting fatigue damage throughout the operating wind speed range, which are calculated via Equations 5 to 7, are presented in Table D2 and illustrated in Figure 6. Four levels, namely, highest, high, low, and lowest, are defined based on the ranking sequence. The pinion gear in the third stage is observed to have both the highest tooth bending and the highest pitting fatigue damage. The primary reason is the large number of cycles that are experienced by this gear. Additionally, the sun gear in the first stage has the highest tooth pitting fatigue damage, which is mainly due to the high tooth contact stress that is caused by the small sun gear tooth curvature. In addition, the lowest gear tooth pitting fatigue damage occurs on the two planetary stage ring gears, which is due to the material resistance for the ring gears being less than those of the other gears.

4.5.2 | Bearing fatigue damage

Figure D2 presents the bearing equivalent load bins with the corresponding number of cycles for bearings INP-A and HS-B at the wind speed of 12.6 m/s. The 20-year bearing fatigue damage is calculated via Equations (7) to (9), and the results are presented in Table D3 and Figure 7. The highest fatigue damage is located at the upwind main bearing INP-A, which is because this bearing withstands huge nontorque loads from the rotor blades. The fatigue damage of this bearing exceeds the limited value of 1 in this case study because of the bearing database limitation; thus, the cooperative studies with bearing manufacturers are suggested for custom bearings. Bearing HS-B incurs the highest fatigue damage, which is mainly due to the large number of load cycles that are experienced by this bearing. In addition, the fatigue damage differs among bearings because of the geometrical restrictions and bearing database limitations; for example, the planet bearing IMS-PL-B in the second stage and IMS-B in the intermediate shaft incur the highest fatigue damage, while IMS-PLC-A in the second planet carrier incurs the lowest fatigue damage.

4.5.3 | Drivetrain vulnerability map

Based on the 20-year gear and bearing fatigue damages, a drivetrain vulnerability map is established by ranking those components according to their damage levels, as shown in Figure 8. According to Table D2 and Figure 6, the gear tooth bending fatigue damage is much more severe

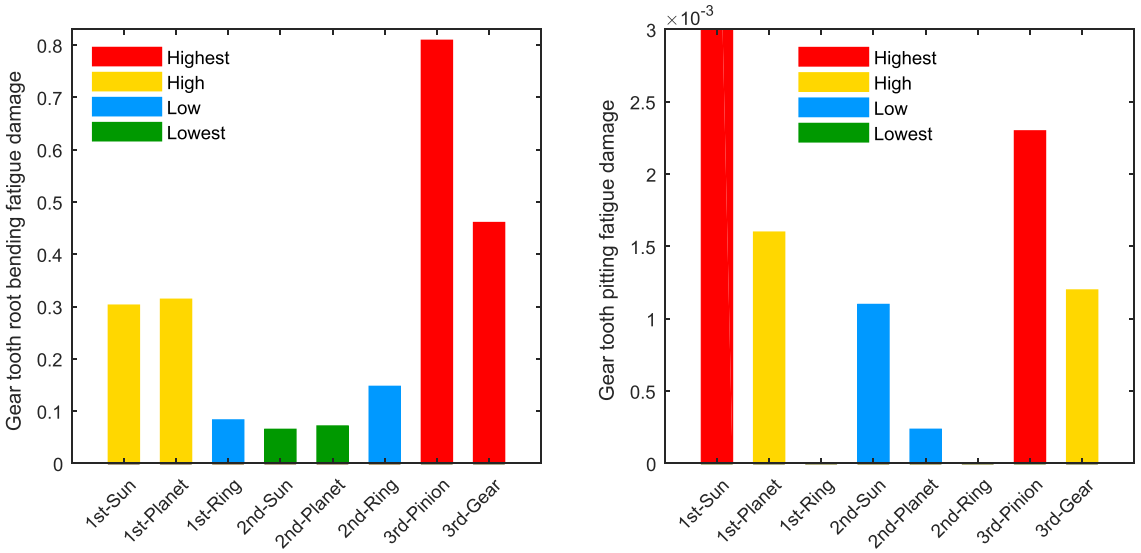

FIGURE 6 20-year gear tooth bending and pitting fatigue damage [Colour figure can be viewed at wileyonlinelibrary.com]

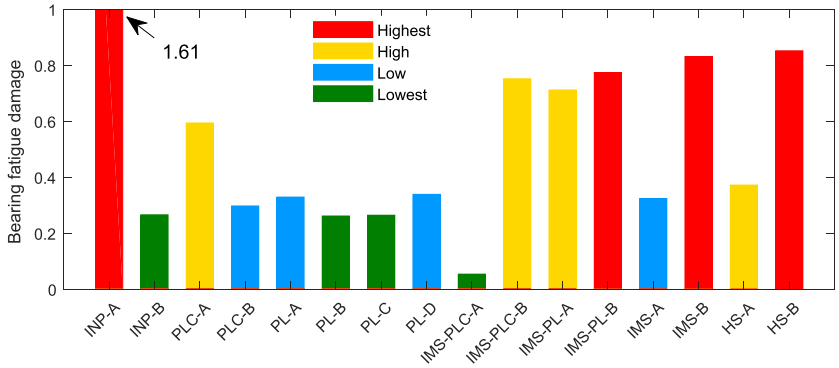

FIGURE 7 20-year bearing fatigue damage [Colour figure can be viewed at wileyonlinelibrary.com]

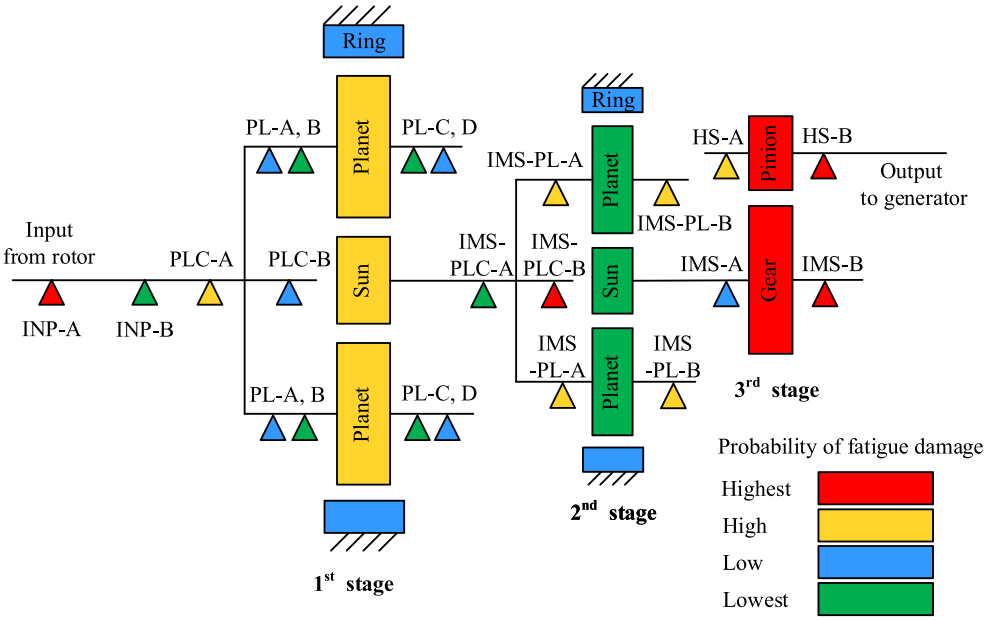

FIGURE 8 10-MW wind turbine drivetrain vulnerability map [Colour figure can be viewed at wileyonlinelibrary.com]

than the pitting fatigue damage, which accords with the conclusion in the study of Niemann et al[55] that gear tooth breakage occurs more easily than gear tooth pitting. Thus, the gear tooth bending fatigue damage is applied in this vulnerability map. The probabilities of fatigue damage of the gears and bearings in the drivetrain model differ. This is primarily due to the geometrical restrictions of the structure, the differences in the materials and in the number of loads cycles, and bearing database limitations.

The drivetrain vulnerability map ranks components from highest to lowest fatigue damage, which could facilitate drivetrain performance assessment and model optimization. The drivetrain inspection and maintenance costs could be approximated by developing an inspection and maintenance strategy that is based on the vulnerability map. Moreover, one can improve the drivetrain design or enhance its reliability by optimizing the components that have the highest fatigue damage, which could substantially reduce the optimization strategy developing time. The vulnerability map of the 10-MW drivetrain differs substantially from that of the 5-MW drivetrain that is presented in the study of Nejad et al,[9] which is due to factors such as the wind turbine rating, drivetrain transmission ratio, and mechanical component materials. Hence, the drivetrain fatigue damage will primarily depend on the loads and load cycles that are experienced by the mechanical components and is not closely rated to the drivetrain layout.

5 | CONCLUDING REMARKS

This paper deals with the design, modelling, and analysis of a medium-speed drivetrain for the DTU 10-MW wind turbine. Detailed design and dynamic modelling parameters are provided for public use to facilitate research on the dynamics of 10-MW wind turbines. The main contributions are summarized as follows:

- A four-point support drivetrain configuration is selected. Several potential gearbox design layouts for the 10-MW wind turbine case study are proposed. The pros and cons of the conventional gearbox layout and several novel gearbox layouts, such as power splitting gearbox layout and compound, differential or double-helix planetary gearbox layout, are discussed and compared. A conventional three-stage gearbox layout is eventually selected to be designed with the intent of providing a benchmark model for public use.
- A detailed drivetrain design methodology is described. The drivetrain components are designed based on the design loads and criteria that are recommended in relevant international standards, and an iterative process is conducted to optimize the drivetrain design via the considerations of its weight, volume, and load sharing performance.
- A high-fidelity drivetrain dynamic model is established via the MBS modelling approach. The properties of this model well accord with those of the simplified drivetrain model that was suggested by DTU. A resonance analysis of the drivetrain model is conducted by utilizing the Campbell diagram and the modal energy distribution of the components and the results demonstrate that the resonance phenomenon does not occur in this model within the normal operating range.
- Global analysis and local drivetrain dynamic analysis in different environmental conditions are conducted. The 20-year gear and bearing fatigue damages are calculated based on stress or equivalent load duration distribution, the Palmgren-Miner linear accumulative damage hypothesis, and long-term environmental condition distributions. A vulnerability map is established by ranking the drivetrain components from highest to lowest fatigue damage level to facilitate the assessment of the inspection and maintenance and the model optimization.

It is noted that the drivetrain design is conducted via only fatigue limit state evaluation in the present study. Further studies on the evaluations of the ultimate limit state (ULS) and the accidental limit state (ALS) are to be conducted in the future. Moreover, the resonance evaluation of the drivetrain model is only conducted in the torsional direction in this study. It is important to evaluate the drivetrain resonance for all modes in the future. The bedplate will be treated as a flexible body, and coupled rotor-bedplate-drivetrain modes will be considered. Then, the drivetrain resonance response will be assessed under nontorque load excitation.

ACKNOWLEDGEMENTS

The first author would like to thank and acknowledge the financial support from the China Scholarship Council (CSC) (grant no. 201706050147).

ORCID

Shuaishuai Wang https://orcid.org/0000-0002-9155-9357
Amir R. Nejad https://orcid.org/0000-0003-0391-8696

REFERENCES

1. Bak C, Zahle F, Bitsche R, et al. Description of the dtu 10 mw reference wind turbine. *DTU Wind Energy Report-I-0092*. 2013;5.
2. Cox K, Echtermeyer A. Structural design and analysis of a 10 mw wind turbine blade. *Energy Procedia*. 2012;24:194–201.
3. Smilden E, Bachynski EE, Sørensen AJ, Amdahl J. Site-specific controller design for monopile offshore wind turbines. *Marine Struct*. 2018;61:503–523.
4. Velarde J, Bachynski EE. Design and fatigue analysis of monopile foundations to support the dtu 10 mw offshore wind turbine. *Energy Procedia*. 2017;137:3–13.
5. Guo Y, Keller J, LaCava W. Combined effects of gravity, bending moment, bearing clearance, and input torque on wind turbine planetary gear load sharing. Tech. Rep., Golden, CO (United States), National Renewable Energy Lab.(NREL); 2012.
6. Dong W, Xing Y, Moan T, Gao Z. Time domain-based gear contact fatigue analysis of a wind turbine drivetrain under dynamic conditions. *Int J Fatigue*. 2013;48:133–146.
7. Jiang Z, Xing Y, Guo Y, Moan T, Gao Z. Long-term contact fatigue analysis of a planetary bearing in a land-based wind turbine drivetrain. *Wind Energy*. 2015;18(4):591–611.
8. Xing Y, Karimirad M, Moan T. Modelling and analysis of floating spar-type wind turbine drivetrain. *Wind Energy*. 2014;17(4):565–587.
9. Nejad AR, Guo Y, Gao Z, Moan T. Development of a 5 mw reference gearbox for offshore wind turbines. *Wind Energy*. 2016;19(6):1089–1106.
10. Areva 5 MW wind turbine. https://en.wind-turbine-models.com/turbines/23-areva-m5000-116. Accessed April 06, 2018.
11. V162-5.6 MW wind turbine. https://www.vestas.com/en/products/enventus_platform#!enventus-platform. Accessed December 06, 2019.
12. V174-9.5 MW and v164-10.0 MW wind turbines. http://www.mhivestasoffshore.com/innovations/. Accessed December 06, 2019.
13. Jonkman J, Butterfield S, Musial W, Scott G. Definition of a 5-mw reference wind turbine for offshore system development. Tech. Rep., Golden, CO (United States), National Renewable Energy Lab.(NREL); 2009.
14. Nejad AR, Bachynski EE, Li L, Moan T. Correlation between acceleration and drivetrain load effects for monopile offshore wind turbines. *Energy Procedia*. 2016;94:487–496.
15. Johannessen K, Meling TS, Haver S, et al. Joint distribution for wind and waves in the northern north sea. *Int J Offshore Polar Eng*. 2002;12(1):1053-5381.
16. Ronold KO, Larsen GC. Variability of extreme flap loads during turbine operation. In: European Wind Energy Conference and Exhibition James and James Science Publishers; 1999; London, UK:224–227.
17. IEC61400-3. Wind turbines, part 3: Design requirements for offshore wind turbines. International Electrotechnical Commission: Geneva, Switzerland; 2009.
18. Sima. Simulation of marine operation. https://www.sintef.no/en/software/sima. Accessed July 07, 2018.
19. Nejad AR, Gao Z, Moan T. Long-term analysis of gear loads in fixed offshore wind turbines considering ultimate operational loadings. *Energy Procedia*. 2013;35:187–197.
20. Xing Y, Karimirad M, Moan T. Effect of spar-type floating wind turbine nacelle motion on drivetrain dynamics. European Wind Energy Association annual event, Copenhagen; 2012.
21. IEC61400-4. Wind turbines, part 4: Standard for design and specification of gearboxes. International Electrotechnical Commission: Geneva, Switzerland; 2012.
22. IEC61400-1. Wind turbines, part 1: Design requirements. International Electrotechnical Commission: Geneva, Switzerland; 2005.
23. DNVGL-ST-0361. Machinery for wind turbines. Det Norske Veritas Germanischer Lloyd; 2016.
24. Torsvik J, Nejad AR, Pedersen E. Main bearings in large offshore wind turbines: development trends, design and analysis requirements. *J Phys Conf Ser*. 2018;1037(4):42020.
25. Schmidt S, Vath A. Comparison of existing medium-speed drive train concepts with a differential gearbox approach. *Euro Wind Energy Assoc*. Copenhagen; 2012:179–186.
26. Guo Y, Keller JA. Rolling element bearing dynamics in wind turbines. tech. rep., Golden, CO (United States), National Renewable Energy Lab.(NREL); 2019.
27. Guo Y, Sheng S. Probability of failure for gearbox high-speed-stage bearings in wind turbines. Tech. Rep., Golden, CO (United States), National Renewable Energy Lab.(NREL); 2018.
28. Wang S, Nejad AR, Bachynski EE, Moan T. A comparative study on dynamic behaviours of 10-MW conventional and compact gearboxes for offshore wind turbines. *Submitted to the J Renew Energy*.

29. Wang S, Nejad AR, Moan T. Design and dynamic analysis of a compact 10 MW medium speed gearbox for offshore wind turbines. In: Accepted in proceedings of the international offshore wind technical conference (IOWTC) St. Julian's, Malta; 2019.
30. Wang S, Zhu C, Song C, Liu H, Tan J, Bai H. Effects of gear modifications on the dynamic characteristics of wind turbine gearbox considering elastic support of the gearbox. *J Mech Sci Technol*. 2017;31(3).
31. ISO6336-2. Calculation of load capacity of spur and helical gears, part 2: calculation of surface durability (pitting). International Organization for Standardization: Geneva, Switzerland; 2006.
32. ISO6336-3. Calculation of load capacity of spur and helical gears, part 3: calculation of tooth bending strength. International Organization for Standardization: Geneva, Switzerland; 2006.
33. ISO6336-6. Calculation of load capacity of spur and helical gears, part 6: calculation of service life under variable load. International Organization for Standardization: Geneva, Switzerland; 2006.
34. ISO281. Rolling bearings-dynamic load ratings and rating life. International Organization for Standardization: Geneva, Switzerland; 2007.
35. DIN743. Calculation of load capacity of shafts and axles, part 4: Fatigue limit, endurance limit - equivalently damaging continuous stress, Germany, German Institute for Standardization; 2012.
36. Kisssoft. Design software for mechanical engineering applications. http://www.kisssoft.ch/english/home/index.php. Accessed August 03, 2018.
37. Wang S, Nejad AR, Moan T. On initial design and modelling of a 10 MW medium speed drivetrain for offshore wind turbines. *J Phys Conf Ser*; 1356(2019):12024.
38. Simpack. Multi body system software. http://www.simpack.com. Accessed November 16, 2018.
39. Guo Y, Keller J, LaCava W. Planetary gear load sharing of wind turbine drivetrains subjected to non-torque loads. *Wind Energy*. 2015;18(4):757–768.
40. LaCava W, Xing Y, Guo Y, Moan T. Determining wind turbine gearbox model complexity using measurement validation and cost comparison. Tech. Rep., Golden, CO (United States), National Renewable Energy Lab.(NREL); 2012.
41. Nejad AR, Xing Y, Guo Y, Keller J, Gao Z, Moan T. Effects of floating sun gear in a wind turbine's planetary gearbox with geometrical imperfections. *Wind Energy*. 2015;18(12):2105–2120.
42. Helsen J, Vanhollebeke F, Marrant B, Vandepitte D, Desmet W. Multibody modelling of varying complexity for modal behaviour analysis of wind turbine gearboxes. *Renew Energy*. 2011;36(11):3098–3113.
43. Peeters JL, Vandepitte D, Sas P. Analysis of internal drive train dynamics in a wind turbine. *Wind Energy Int J Prog Appli Wind Power Convers Technol*. 2006;9(1-2):141–161.
44. Xing Y, Moan T. Multi-body modelling and analysis of a planet carrier in a wind turbine gearbox. *Wind Energy*. 2013;16(7):1067–1089.
45. Guo Y, Keller J, La Cava W, Austin J, Nejad A, Halse C, Bastard L, Helsen J. Recommendations on model fidelity for wind turbine gearbox simulations. Tech. Rep., Golden, CO (United States), National Renewable Energy Lab.(NREL); 2015.
46. ISO6336-1. Calculation of load capacity of spur and helical gears, part 6: basic principles, introduction and general influence factors. International Organization for Standardization: Geneva, Switzerland; 2006.
47. Romax. Romaxwind software. https://romaxtech.com. Accessed October 06, 2018.
48. Nejad AR, Gao Z, Moan T. On long-term fatigue damage and reliability analysis of gears under wind loads in offshore wind turbine drivetrains. *Int J Fatigue*. 2014;61:116–128.
49. Wilkins E. *Cumulative damage in fatigue*, Colloquium on Fatigue/Colloque de Fatigue/Kolloquium über Ermüdungsfestigkeit. Berlin, Heidelberg: Springer; 1956;321–332.
50. ISO6336-5. Calculation of load capacity of spur and helical gears, part 5: strength and quality of materials. International Organization for Standardization: Geneva, Switzerland.
51. Nejad AR, Gao Z, Moan T. Fatigue reliability-based inspection and maintenance planning of gearbox components in wind turbine drivetrains. *Energy Procedia*. 2014;53:248–257.
52. Nejad AR. Modelling and analysis of drivetrains in offshore wind turbines. In: Anaya-Lara O, Tande JO, Uhlen K, Merz K, eds. *Offshore wind energy technology*,. Hoboken, N.J.: Wiley Online Library; 2018:37–101.
53. Oyague F. Gearbox modeling and load simulation of a baseline 750-kw wind turbine using state-of-the-art simulation codes. Tech. Rep., Golden, CO (United States), National Renewable Energy Lab.(NREL); 2009.
54. Guo Y, Parker RG. Sensitivity of general compound planetary gear natural frequencies and vibration modes to model parameters. *J Vib Acoust*. 2010;132(1):11006.
55. Niemann G, Winter H. *Maschinenelemente. Band ii: Getriebe allgemein, zahnradgetriebe–grundlagen, stirnradgetriebe*: Springer-Verlag; 1983.

How to cite this article: Wang S, Nejad AR, Moan T. On design, modelling, and analysis of a 10-MW medium-speed drivetrain for offshore wind turbines. *Wind Energy*. 2020;23:1099–1117. https://doi.org/10.1002/we.2476

APPENDIX A: DRIVETRAIN DESIGN PARAMETERS

TABLE A1 10-MW wind turbine drivetrain specifications

Parameter	Value
Drivetrain type	Four-point support
Gearbox type	Two planetary + one parallel
First stage ratio	4.423
Second stage ratio	5.192
Third stage ratio	2.179
Total ratio	50.039
Designed power (MW)	10
Rated input shaft speed (rpm)	9.6
Rated generator shaft speed (rpm)	480.4
Rated input shaft torque (KN.m)	9947.9
Rated generator shaft torque (KN.m)	198.8
Drivetrain dry mass (× 1000 kg)	141.54
Gearbox dry mass (× 1000 kg)	60.43
Gearbox maximum outer diameter (m)	3.098
Designed service life (y)	20

TABLE A2 Material parameters of main components

Components	Material	Density(Kgm^{-3})	Young Modulus (GPa)	Poisson Ratio
Hub	QT400	7010	161	0.274
Planet carrier	QT700	7090	169	0.305
Planet/Sun gears	18CrNiMo7-6	7800	207	0.300
Ring gears	42CrMo4	7800	207	0.300
Shafts	18CrNiMo7-6	7800	207	0.300

TABLE A3 Geometrical specification of gears

Parameter	FirstStage	SecondStage	ThirdStage
Type	Planetary	Planetary	Parallel
Ratio	1:4.423	1:5.192	1:2.179
Number of planets	5	3	–
Normal module (mm)	30	20	18
Normal pressure angle (degree)	20	20	20
Helix angle (degree)	8	8	12
Face width (mm)	800	520	500
Centre distance (mm)	877.033	684.273	825.885
Number of teeth, Sun/Pinion	26	26	28
Number of teeth, Planet/Gear	31	41	61
Number of teeth, Ring gear	89	109	–
Profile shift coefficient, Sun/Pinion	0.2702	0.2787	0.2976
Profile shift coefficient, Planet/Gear	0.2093	0.1213	0.1024
Profile shift coefficient, Ring gear	−0.1591	−0.0024	–
Pitch diameter (mm), Sun/Pinion	787.666	525.110	515.260
Pitch diameter (mm), Planet/Gear	939.140	828.059	1122.530
Pitch diameter (mm), Ring gear	2696.240	2201.424	–
Tip diameter (mm), Sun/Pinion	863.878	576.258	561.973
Tip diameter (mm), Planet/Gear	1011.698	872.911	1162.216
Tip diameter (mm), Ring gear	2645.786	2161.52	–
Root diameter (mm), Sun/Pinion	719.878	480.258	475.573
Root diameter (mm), Planet/Gear	867.689	776.911	1075.816
Root diameter (mm), Ring gear	2780.786	2251.520	–

Name	Type	Designation	Provider	OD	ID	B
INP-A	TRB	2TR1450	Koyo	1770	1450	145
INP-B	TRB	2TR950B	Koyo	1250	950	136
PLC-A	TRB	LL889049/LL889010D	Koyo	1435	1270	146
PLC-B	CRB	NNU49/1120-S-M-C3	FAG	1460	1120	335
PL-A,B,C,D	TRB	45T806520D	Koyo	650	400	200
IMS-PLC-A	TRB	2TR950B	Koyo	1250	950	136
IMS-PLC-B	TRB	452/900	Koyo	1280	900	140
IMS-PL-A,B	TRB	45368	Koyo	580	340	190
IMS-A	TRB	2TR600J	Koyo	870	600	134.5
IMS-B	TRB	452/500	Koyo	720	500	83.5
HS-A	CRB	NNCF4980BV	SKF	540	400	140
HS-B	TRB	45T605729	Koyo	570	300	290

Note. TRB, tapered roller bearing; CRB, cylindrical roller bearing; OD/ID, outer/inner diameter; B, bearing thickness. All dimensions are metric (millimetre).

TABLE A4 Designation and geometrical specification of bearings

APPENDIX B: DRIVETRAIN MULTIBODY SYSTEM MODELLING PARAMETERS

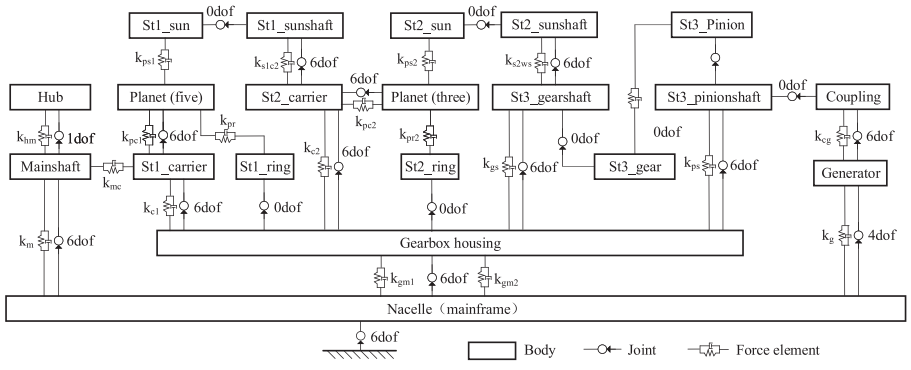

FIGURE B1 Topological diagram of the 10-MW offshore wind turbine drivetrain

Components	Mass (Kg)	$I_{xx}(Kgm^2)$	$I_{yy}(Kgm^2)$	$I_{zz}(Kgm^2)$
Hub	227962.0	156699761.4	80000000	80000000
Main shaft	58479.5	17878.6	157739.7	157739.7
St1-planet carrier	25360.2	19314.1	18029.5	18029.6
St1-sun shaft	1731.1	359.5	1002.0	1002.0
St2-planet carrier	10475.4	4873.7	3871.9	3871.8
St2-sun shaft	371.7	39.5	117.1	117.1
St3-wheel shaft	5849.2	679.0	727.6	765.4
St3-pinion shaft	1797.9	40.9	568.7	568.7
St1-ring gear	10184.2	21272.4	11179.3	11179.4
St1-planet gear	2353.7	393.0	554.3	554.3
St1-sun gear	2653.1	242.7	309.7	309.7
St2-ring gear	4176.8	5744.5	2966.3	2966.4
St2-planet gear	989.6	133.9	148.7	148.7
St2-sun gear	776.3	31.8	39.1	39.1
St3-wheel gear	3760.0	613.1	390.0	390.0
St3-pinion gear	854.5	29.5	33.3	33.3

Abbreviation: St, Stage.

TABLE B1 Mass and inertia moments specifications of main components

TABLE B2 Dynamic model parameters of bearings

Name	K_x(N/m)	K_y(N/m)	K_z(N/m)	K_β(Nm/rad)	K_γ(Nm/rad)
INP-A	4.1442×10^9	1.0231×10^{10}	1.4984×10^{10}	1.4506×10^9	9.8937×10^8
INP-B	4.0095×10^9	6.8461×10^9	9.9126×10^9	6.691×10^8	6.691×10^8
PLC-A	7.7772×10^9	2.2339×10^{10}	3.1137×10^{10}	2.642×10^9	1.8946×10^9
PLC-B	0	1.3445×10^{10}	2.0185×10^{10}	1.4678×10^8	9.6695×10^7
PL-A,B,C,D	6.2541×10^9	8.0297×10^9	1.0761×10^{10}	1.0116×10^8	7.4871×10^7
IMS-PLC-A	2.15469.2936$\times10^9$	9.2936×10^8	8.0765×10^9	5.2667×10^8	5.9859×10^7
IMS-PLC-B	3.1836×10^9	2.3904×10^{10}	2.3694×10^{10}	4.1821×10^8	4.2283×10^8
IMS-PL-A,B	7.6453×10^8	7.3226×10^9	9.6458×10^9	2.7065×10^6	1.5687×10^6
IMS-A	9.5783×10^8	6.3441×10^9	9.1733×10^9	5.9894×10^7	4.1182×10^7
IMS-B	1.5269×10^9	1.1778×10^{10}	1.1051×10^{10}	6.0533×10^7	6.4727×10^7
HS-A	0	2.5422×10^9	1.1793×10^{10}	1.6331×10^8	3.3156×10^7
HS-B	1.3427×10^9	8.6946×10^9	1.0694×10^{10}	1.6677×10^8	1.3047×10^8

APPENDIX C: GLOBAL LOAD AND MOTION RESPONSE

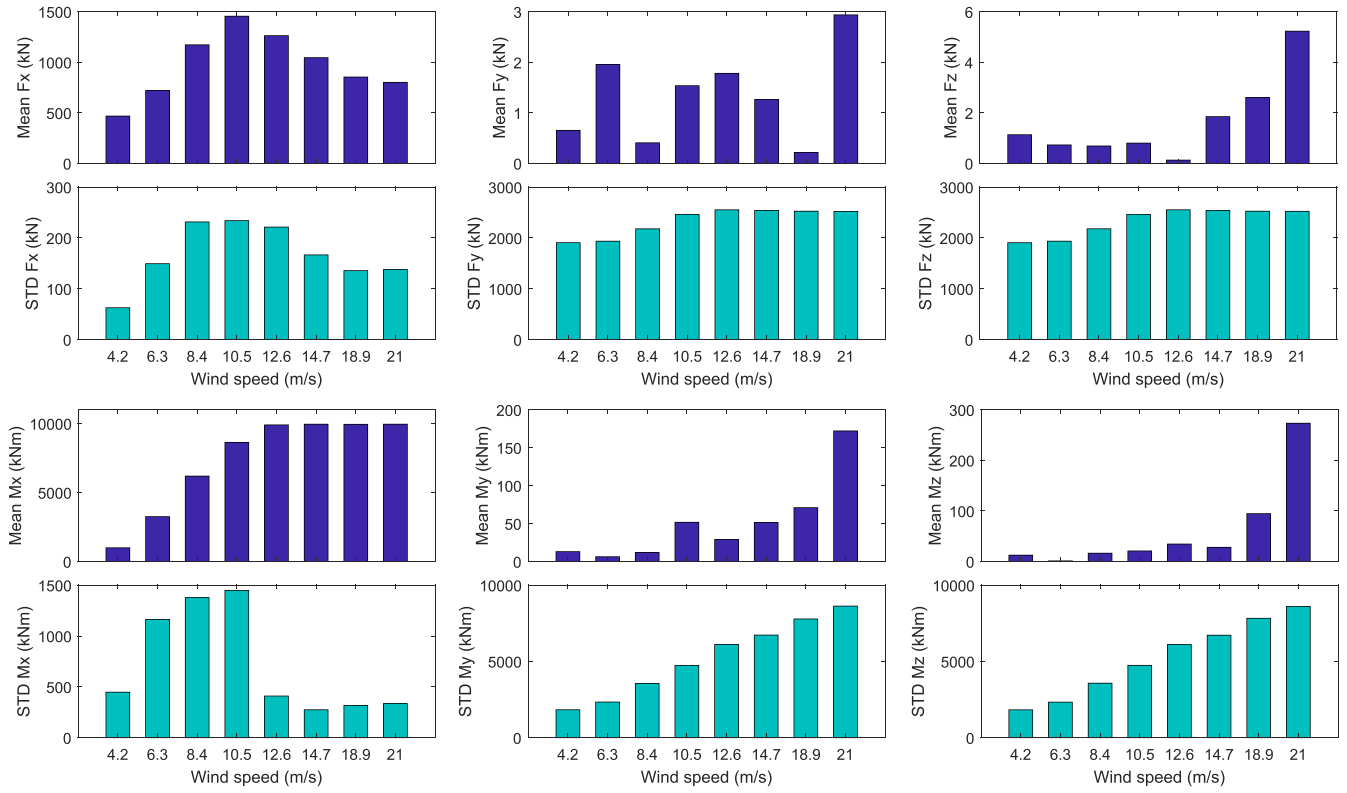

FIGURE C1 Mean and standard deviation of forces and moments applied at hub centre [Colour figure can be viewed at wileyonlinelibrary.com]

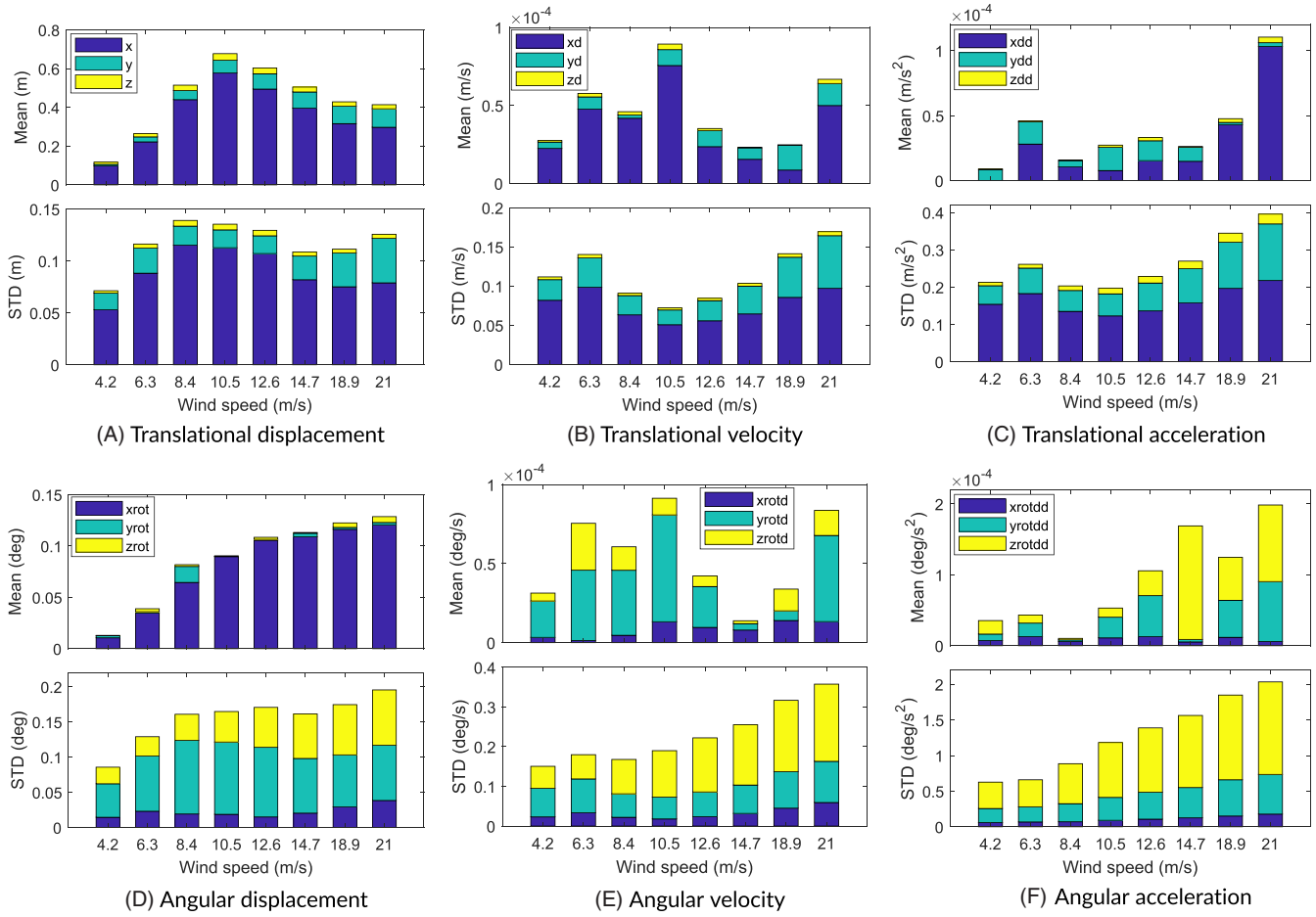

FIGURE C2 Nacelle motions applied on mainframe [Colour figure can be viewed at wileyonlinelibrary.com]

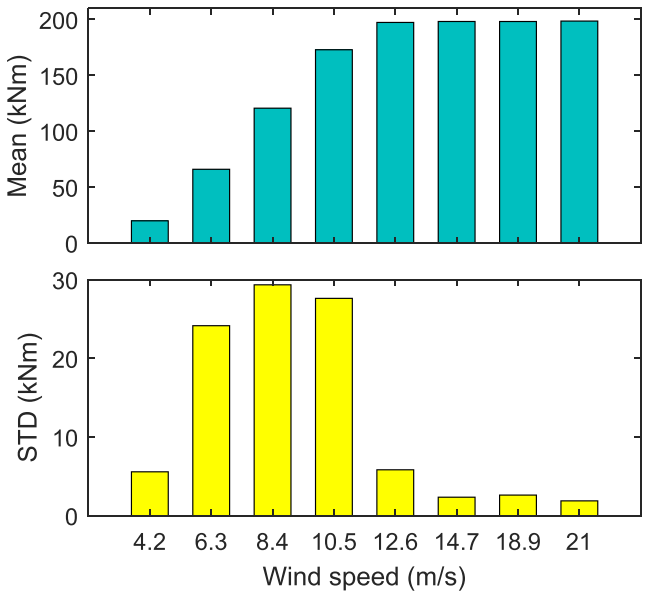

FIGURE C3 Mean and standard deviation of generator torque [Colour figure can be viewed at wileyonlinelibrary.com]

APPENDIX D: DRIVETRAIN FATIGUE DAMAGE

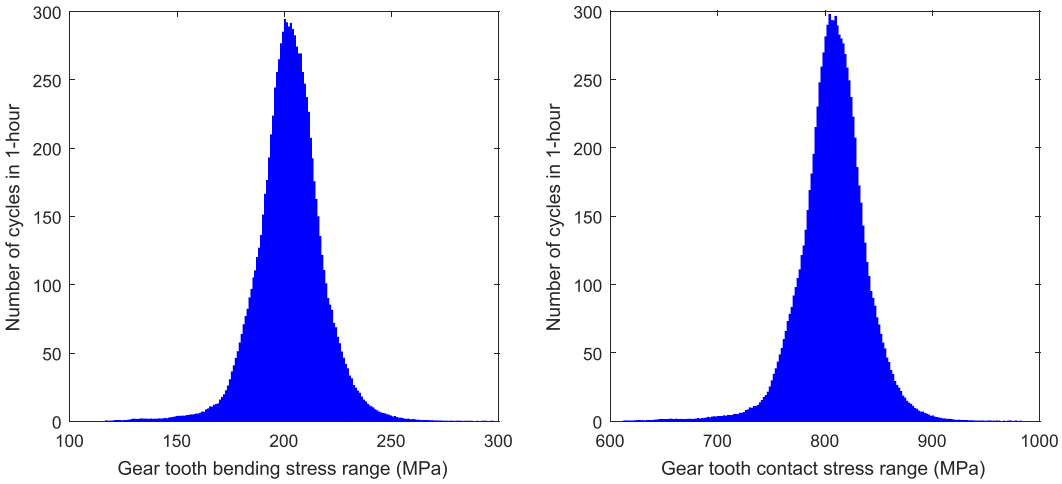

FIGURE D1 First sun gear tooth bending stress and contact stress bins at 12.6-m/s wind speed [Colour figure can be viewed at wileyonlinelibrary.com]

TABLE D1 Gear bending and pitting fatigue SN curve parameters

Stage	Gear	Bending Fatigue		Pitting Fatigue	
		m	k	m	k
	Sun gear	6.901	2.372×10^{26}	14.670	3.876×10^{54}
First stage	Planet gear	6.955	3.393×10^{26}	14.670	3.876×10^{54}
	Ring gear	7.023	2.453×10^{25}	16.404	3.230×10^{55}
	Sun gear	7.171	2.208×10^{27}	15.231	3.051×10^{56}
Second stage	Planet gear	7.312	5.655×10^{27}	15.231	3.051×10^{56}
	Ring gear	7.330	5.568×10^{26}	18.672	3.126×10^{62}
Third stage	Pinion	7.115	1.804×10^{27}	16.376	2.256×10^{60}
	Gear	7.194	3.072×10^{27}	16.376	2.256×10^{60}

TABLE D2 20-year gear pitting and bending fatigue damage

Stage	Gear	D_b	D_p
First stage	Sun gear	0.3030	0.0094
	Planet gear surface1	0.1301	2.2679×10^{-7}
	Planet gear surface2	0.3143	0.0016
	Ring gear	0.0835	7.5767×10^{-8}
Second stage	Sun gear	0.0655	0.0011
	Planet gear surface1	0.0217	2.9769×10^{-9}
	Planet gear surface2	0.0719	2.3715×10^{-4}
	Ring gear	0.1477	2.8410×10^{-10}
Third stage	Pinion	0.8095	0.0023
	Gear	0.4610	0.0012

Note. D_b, gear tooth bending fatigue damage; D_p, gear tooth pitting fatigue damage; Planet gear surface1, planet gear surface meshing with ring gear; Planet gear surface2, planet gear surface meshing with sun gear.

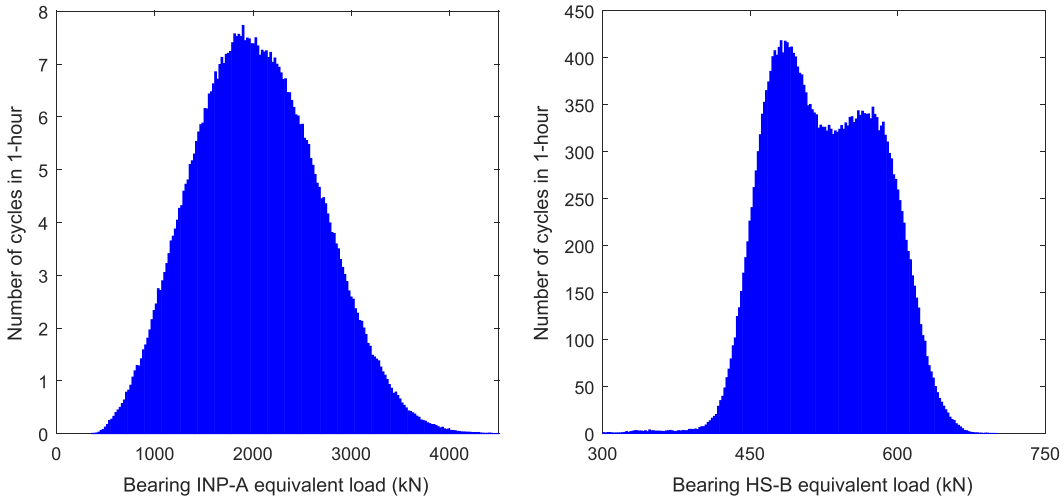

FIGURE D2 Bearing equivalent load bins, INP-A (left) and HS-B (right) [Colour figure can be viewed at wileyonlinelibrary.com]

TABLE D3 20-year bearing fatigue damage

Stage	Bearing	D
Main shaft	INP-A	1.6064
	INP-B	0.2660
First stage	PLC-A	0.5941
	PLC-B	0.2976
	PL-A	0.3293
	PL-B	0.2617
	PL-C	0.2645
	PL-D	0.3391
Second stage	IMS-PLC-A	0.054
	IMS-PLC-B	0.7521
	IMS-PL-A	0.7120
	IMS-PL-B	0.7744
Third stage	IMS-A	0.3244
	IMS-B	0.8314
	HS-A	0.3723
	HS-B	0.8519